Molecular modelling of TLR agonist Pam3CSK4 entrapment in PLA nanoparticles as a tool to explain loading efficiency and functionality

Myriam Lamrayah, Fanny Charriaud, Shangnong Hu, Simon Megy, Raphael Terreux, Bernard Verrier

Molecular modelling of TLR agonist Pam_3CSK_4 entrapment in PLA nanoparticles as a tool to explain loading efficiency and functionality

Myriam Lamrayah[a*], Fanny Charriaud[a], Shangnong Hu[ab], Simon Megy[ab], Raphael Terreux[ab], Bernard Verrier[a]

[a] Colloidal vectors and tissue transport, UMR5305, LBTI, Institut de Biologie et Chimie des Protéines, Université Lyon 1, 7 Passage du Vercors, 69367 Lyon Cedex 07, France

[b] Pôle Rhône-Alpes de Bioinformatique - Lyon Gerland, UMR5305, LBTI, Institut de Biologie et Chimie des Protéines, Université Lyon 1, 7 Passage du Vercors, 69367 Lyon Cedex 07, France

* Corresponding author.
E-mail address: myriam.lamrayah@ibcp.fr

Designing potent and safe-of-use therapies against cancers and infections remains challenging despite the emergence of novel molecule classes like checkpoint inhibitors or Toll-Like-Receptor ligands. The latest therapeutic perspectives under development for immune modulator administration exploits vectorization, and biodegradable delivery systems are one of the most promising vehicles. Nanoparticles based on Poly (D,L) Lactic Acid (PLA) as polymer for formulation are widely investigated due to its bioresorbable, biocompatible and low immunogen properties. We propose a PLA-based nanoparticle delivery system to vectorize Pam_3CSK_4, a lipopeptide TLR1/2 ligand and a potent activator of the proinflammatory transcription factor NF-κB that shows a self-assembling behavior from 30 µg/mL onwards. We demonstrate successful encapsulation of Pam_3CSK_4 in PLA nanoparticles by nanoprecipitation in a 40-180 µg/mL concentration range, with 99% of entrapment efficiency. By molecular modelling, we characterize drug/carrier interactions and conclude that Pam_3CSK_4 forms clusters onto the nanoparticle and is not encapsulated into

the hydrophobic core. *In silico* predictions provide nanoprecipitation optimization and the mechanistic understanding of the particle dynamics. The loaded-Pam_3CSK_4 maintains bioactivity on TLR2, confirmed by *in vitro* experiments using reporter cell line HEK-Blue hTLR2. Our presented data and results are convincing evidence that Pam_3CSK_4-loaded in PLA nanoparticles represent a promising immune modulating system.

PLA nanoparticles, Toll-Like-Receptor, Pam_3CSK_4, immune modulation, molecular modelling, binding specificity

PLA: poly(D,L) lactic acid; NP: nanoparticles; PLA-NP: nanoparticles of poly(D,L) lactic acid; TLR: toll-like receptor; PRR: pattern recognition receptor; PAMP: pathogen-associated molecular patterns; DDS: drug delivery system; CAC: critical aggregation concentration; DPD: dissipative particle dynamics; MAb: monoclonal antibody; BP: binding potential.

1. Introduction

Biodegradable delivery systems are generating a substantial amount of interest in the therapeutic field, particularly in cancerology and infectiology (Banik et al., 2016). Amongst the latest innovative systems, Poly(D,L) Lactic Acid (PLA) nanoparticles (NP) are one of the most promising vectors (Peres et al., 2017). Due to its bioresorbability, biocompatibility and low immunogenicity, PLA polymer has been approved for human use in tissue engineering scaffolds, medical or cosmetic implants, and as component of delivery carriers for numerous preclinical candidates (Tyler et al., 2016). Our growing expertise has enabled us to investigate the potential of PLA-NP as vaccine delivery platforms (Coolen et al., 2019; Dalzon et al., 2016; Rességuier et al., 2017), immunotherapy tools (Pavot et al., 2013), and inflammatory skin diseases treatment after their entrapment in hydrogel (Boisgard et al., 2017), all the while controlling PLA-NP toxicity (Legaz et al., 2016). Despite the increasing financial investment in nanotechnologies (Dong et al., 2019), very few have reached the ultimate marketing authorization (Ragelle et al., 2017). The booming of performing analytical tools, mainly microscopy techniques and molecular modelling approaches, is facilitating the further understanding of the molecular mechanism underlying these therapeutic strategies. For instance, dynamic molecular simulations offer new perspectives to estimate content-contained interactions in delivery systems. In parallel, regulations for nanomaterials are being reinforced by the authorities, imposing to the scientific community a more thorough description and work ethic of their products (Miernicki et al., 2019). This article considers the use of cutting edge techniques for a precise comprehension of the chemical and molecular properties of unique PLA-NP loaded with an immune modulating component.

Designing potent and safe-of-use therapies against cancers and infections has become a challenge. Both the innate and adaptive immune systems must be targeted as they play essential roles in the pathogenesis. Latest findings show immunotherapies are the future treatments against these medical outbreaks (Riley et al., 2019). This is supported by the

emergence of new molecule subclasses and the increasing number of drug approvals accorded to checkpoint inhibitors, monoclonal antibodies or Toll-Like Receptor (TLRs) agonists (Hennessy et al., 2010). Mostly found on antigen presenting cells such as dendritic cells, monocytes and macrophages, TLRs are vital receptors that belong to the Pattern Recognition Receptor (PRR) family. PRRs are recognized by Pathogen-Associated Molecular Patterns (PAMP), structural components present on microorganisms. In humans, 10 different TLRs have been identified and are expressed either on the cell surface or inside the endosomes. The type of ligand interacting with each TLR is correlated to the pathogen's capacity of internalization. For example, endosomal TLRs 3, 7, 8 and 9 are bound by viral or bacterial DNA/RNA sequences. Other TLRs are located in cell membranes and are activated by external components of pathogens such as bacterial lipolysaccharide or lipopeptides. Following TLR binding by PAMP, activation of several transcription factors are triggered, including NF-κB and interferon response factors. This stimulates the transcription of proinflammatory agents (IL-6, IL-12, IL-23, TNF-α) essential to the activation of a proper defense mechanism. TLR agonists have been extensively studied as adjuvants to treat cancer (Li et al., 2017) or as specific drug against infections (Mifsud et al., 2014), either in monotherapy or in association with conventional drugs in order to enhance their efficacy via immune cell activation (Lee et al., 2014). These strategies intended to stimulate the patient's immune system have already demonstrated high successful therapeutic results: agonists of TLR4 (Coler et al., 2018), TLR7 (Boni et al., 2018), TLR8 (Chow et al., 2017) and TLR9 (Beeh et al., 2013) have been admitted for clinical trials. However, few issues remain unsolved regarding the harmless use of these ligands. TLR agonists have off-target effects on healthy cells in addition to the expected activity on the diseased organ, making them responsible for large uncontrolled side effects by systemic route, up to autoimmune disorders (Lang et al., 2005). A more recent notable adverse reaction is the potential cytokine storm effect, which jeopardies most of the current attempts to develop efficient immuno-based therapies (Zhao et al., 2019). The cytokine storm includes life-threatening conditions that are manifested by extremely elevated serum cytokine levels and is mostly

mediated by TLR agonists (Reed et al., 2013). Frequent administrations or high doses are non-feasible and thus, a drug delivery system (DDS) must be considered.

Another limit to validate TLR ligands in drug development is their physicochemical properties that contribute to their undesired drug characteristics according to Lipinski's rule of five. The poor bioavailability, short half-life and rapid clearance of peptide or nucleotide-based drugs hinder their potential commercialization (Engel et al., 2011). Thus, key challenges remain in the choice of DDS to deliver *in vivo* such molecules. Studies have suggested the conjugation of TLR agonists as an option to influence pharmacokinetic profiles (Ignacio et al., 2018), but it should not affect the structure-activity relationship. Here, we describe how to overcome these drawbacks by using biodegradable nanovehicles, able to carry such immune modulators and still improving their efficiency through prolonged activity and compliance by reducing side effects (Tacken et al., 2011).

This study focuses on the Pam_3CSK_4 molecule, a synthetic triacylated lipoprotein consisting of a tri-palmitoyl-S-glyceryl cysteine with a pentapeptide SKKKK. Pam_3CSK_4 is a TLR1/2 ligand that mimics the triacylated amino terminus of a bacterial lipopeptide. It is a potent activator of the proinflammatory transcription factor NF-κB, produced after TLR2 recognition and heterodimer formation with TLR1 through their cytoplasmic domain. More precisely, the two ester-bound palmitoyl chains interact with TLR2 binding pocket when the third amine-bound palmitoyl chain interacts with TLR1. Then, TLR1/TLR2 complex connects with the modified glycerol and peptide parts of the ligand by hydrogen bonds (Botos et al., 2011).

Known as a T-cell response inducer, soluble Pam_3CSK_4 has been shown to be beneficial in multiple fields such as neurology (Kim et al., 2015) or virology (Lucifora et al., 2018) and more interestingly, in a chirality-configuration dependent manner (Khan et al., 2009). This lipopeptide also presents the particularity of self-assembling that certainly impacts its bioactivity and therefore could be an obstacle for pharmaceutical development. Hamley *et al* highlighted for the first time the self-assembled structure of TLR ligand lipopeptides containing CSKKKK sequence (Hamley et al., 2014). They showed that Pam_3CSK_4 forms worm-like micelles when the critical aggregation concentration (CAC) of 0.003 wt% is

reached. By using a DDS, electrostatic interaction affinities will be modified, shifting the CAC for higher administrable quantities. In this study, we propose an innovative form of Pam_3CSK_4-loaded PLA-NP capable of bypassing the physicochemical self-assembling phenomenon and maintaining an immune activity. We highlight the added values of vectorization by comparing soluble Pam_3CSK_4 versus loaded forms and we (i) demonstrate that it is possible to experimentally vectorize the candidate lipopeptide even at quantities above its CAC, (ii) investigate entrapment mechanism by *in silico* predictions to understand PLA-NP/ Pam_3CSK_4 interactions, and (iii) show the vectorization does not impact the immune modulatory activity of the molecule. Pam_3CSK_4 loading in PLA-NP will enable the protection of the molecule from proteolytic enzymatic degradation and directly deliver it in the appropriate endocytosing cells, mainly DCs and macrophages. Indeed, particulate entrapment was widely investigated and showed that the internalization is endocytosis-dependent (Behzadi et al., 2017). Via vectorization in PLA-NP, Pam_3CSK_4 side effects will be avoided and the required concentration for a strong immune response will be decreased.

2. Material and methods

2.1. Materials

All reagents used were of analytical grade and received from commercial sources. Acetone and ethanol were purchased from Sigma-Aldrich (St. Louis, MO, USA). Phosphate Buffer Saline (PBS), Dulbecco's Modified Eagle's Medium (DMEM), Fetal Bovine Serum (FBS) and Penicillin/Streptomycin were purchased from Gibco (Thermo Fisher Scientific, Inc., Waltham, MA, USA).

2.2. Cell culture

HEK-Blue™-hTLR2 cells were obtained from Invivogen and cultured in DMEM, supplemented with 10% FBS, Penicillin-Streptomycin (5000 U/mL) in a 37°C incubator (Heracell 150i, Thermo Scientific) under 5% CO2 and 95% humidity. The cells were regularly

sub-cultured via PBS 1X, flushing and tapping. Cell density was determined with Kova cell counting (Glasstic slide, Kova Int, USA).

2.3. PLA-NP preparation

PLA polymer was produced in the laboratory following the patent FR2745005A1 of Phusis (Grenoble, France). PLA-NP were prepared by nanoprecipitation technique as previously described (Lamalle-Bernard et al., 2006). Briefly, the polymer was dissolved in acetone and this solution was added dropwise to an aqueous solution under 250 rpm stirring. Organic solvents were then removed under reduced pressure at 30°C with a Rotavapor R-300 (Buchi, France).

For the entrapment of Pam_3CSK_4 into PLA-NP, the molecule was dissolved in acetone under sonication and agitation before adding with the polymer, to constitute the organic phase. The nanoprecipitation was conducted in the same way, with an aqueous solution made with ethanol and carbonate buffer at a ratio 40:60. The 5 mM carbonate buffer (Na_2CO_3/$NaHCO_3$) was used at a 5 mM concentration (pH 11.0).

The final polymeric concentration was between 40 and 50 mg/mL, depending on the batch, and was measured by weighing the mass of the wet and dried materials. Particulate suspensions were stored at +4 °C.

2.4. Colloidal properties

The average hydrodynamic diameter and size distribution (polydispersity index, PDI) of PLA-NP in suspension were determined by dynamic light scattering at 25°C and a scattering angle of 173°, using a Zetasizer Nano ZS (Malvern, UK). The colloidal suspensions were a hundred time diluted in 0.22 µm filtrated 1 mM NaCl solution. The electrophoretic mobilities (zeta-potential) were measured by laser Doppler velocimetry using the same device, at a scattering angle of 12.5°. Suspensions were a hundred time diluted in 0.22 µm filtrated 1 mM NaCl solution. Measurements were performed immediately and also one month after PLA-NP formulation. Each value was the mean of four independent measurements.

183

184 2.5. Entrapment efficiency (%EE)

185 Ligand concentration was measured with the HEK-Blue™-hTLR2 reporter cell line
186 (InvivoGen) by monitoring the activation of the NF-κB pathway using a secreted embryonic
187 alkaline phosphatase (SEAP) reporter gene. Stimulation of TLR2 ligand activates NF-κB and
188 AP-1, which induces the production of SEAP. The amount of SEAP is quantified with a
189 detection medium that changes color in the presence of alkaline phosphatase. Pam_3CSK_4
190 entrapment efficiencies were obtained through determination of the amount of remaining free
191 ligand in the supernatant after centrifugation of the different PLA-NP formulations (non
192 diluted batches, 15 min at 15000 ×g). Control assays of Pam_3CSK_4 after centrifugation was
193 tested and found homogeneously distributed in supernatant. The supernatants were
194 transferred to 96-well plates (50000 cells/well in triplicate) and cultured for 6-16 hours in
195 presence of a specific SEAP colour substrate, containing all nutrients necessary for cell
196 growth including serum proteins (HEK-Blue™ Detection, InvivoGen). The absorbance of the
197 samples was measured at 620 nm using a microplate reader (BioRad). Free Pam_3CSK_4 (100
198 ng/mL) was used as positive control. The entrapment efficiency (%EE) was determined by
199 measuring the absorbance detected in the supernatant and expressed as percentage of the
200 total amount initially added, based on the following equation:

201 $$Entrapment\ efficiency\ (\%) = (ligand\ mass\ in\ PLA-NP / initial\ ligand\ mass)\ x\ 100$$

202 The absorbance was determined as the mean of three replicates and three independent
203 batches. PBS 1X was used as the negative control. Cell viability was monitored by
204 microscopic observations until the end of the experiment.

205

206 2.6. TLR2 activation by formulations

207 HEK-Blue™-hTLR2 reporter cell line was used as specified above to evaluate Pam_3CSK_4-
208 loaded PLA-NP activity via TLR2 stimulation detection. Briefly, 50000 cells/well were seeded
209 into 96-well plates and stimulated during 10 hours by the different formulations (each batch
210 was diluted for a final polymeric concentration of 0-30 mg/mL in order to fit the standard

curve concentration range). TLR2 activation was monitored by quantifying the amount of SEAP (absorbance at 620 nm). PBS 1X was used as the negative unstimulated control. Monoclonal antibody (MAb) that reacts with mouse TLR2 (MAb-TLR2) was obtained from Invivogen and used for neutralizing control of Pam_3CSK_4 (ref: mab2-mtlr2). Accordingly to the protocol, cells were preincubated with MAb-TLR2 (1 µg/mL) for one hour and then incubated with 20 ng/mL of Pam_3CSK_4.

TLR2 binding potentials of PLA-NP formulations were calculated using the hyperbola standard curve (R^2=0.996) to interpolate free Pam_3CSK_4 curve, and based on the followed equation:

$Y = (Bmax * X)/(Kd + X)$ with X the concentration of the ligand, Y the binding (optical density obtained), Bmax the maximum binding (=0.9326) and Kd the ligand concentration that binds to half the receptor sites at equilibrium (=13.61). TLR2 binding potential (BD%) was calculated by BD%= (obtained BD / expected BD)*100.

2.7. *In silico* simulations

Dissipative Particle Dynamics (DPD) simulations were performed using the Material Studio software (Biovia). For the water molecules (W), we used a coarse graining approach where one bead represents 3 molecules of water. The radius of the water bead was set to 3.23 Å and its molecular mass to 54 Da. Pam_3CSK_4 molecules were constructed using 5 different types of beads: Lysine (K), Serine (S), modified Cysteine (C), modified Glycerol (G), and C_3H_6 fatty acid units (F). PLA molecules were constructed as linear repetitions of 70 units of Lactic Acid monomers $(LA)_n$. For the calculations, all the Flory-Huggins interaction parameters were determined from the solubility parameters d_i, calculated using models constructed with the Amorphous Cell module and calculation were performed with the Forcite module using the COMPASS II force field for atom parameters and partial charges. The Flory-Huggins interaction parameters c_{ij} for the corresponding binary mixtures were calculated using the relation:

238 $c_{ij} = (v/RT)(d_i - d_j)^2$ where R is the gas constant, T the absolute temperature and v is
239 the volume per mole beads (Groot and Rabone, 2001). The molar volumes for each
240 component were determined using the MOE software. The Flory-Huggins interaction
241 parameters were then converted into DPD repulsion parameters $a_{ij,}$ which were obtained
242 using the relation:
243 $a_{ij} = 25 + 3.50\, c_{ij}$ (Groot and Warren, 1997). Calculations were performed using
244 200x200x200 Å cubic periodic boxes of water as starting points for all the dynamics.
245 Droplets with a radius of 85 Å containing a mixture of PLA and Pam_3CSK_4 molecules were
246 placed at their center. In order to mimic the experimental ratio of PLA: Pam_3CSK_4 during the
247 nanoprecipitation, we used mixtures ranging from 1 Pam_3CSK_4 molecules for 600 PLA
248 chains (corresponding to a 20 µg/mL ligand concentration batch) up to 9 Pam_3CSK_4
249 molecules for 600 PLA chains (corresponding to a 180 µg/mL ligand concentration batch).
250 DPD simulations were conducted using various time steps and total simulation times, up to
251 30 ns.
252
253 2.8. Surface morphology by SEM observation
254 PLA-NP observation by Scanning Electron Microscopy (SEM) was performed by adding a
255 drop of blank PLA-NP or Pam_3CSK_4-loaded PLA-NP (180 µg/mL ligand concentration) on a
256 stub, and progressively dried by evaporation under reduced pressure. All samples were then
257 sputtered with a 10 nm gold/palladium layer prior observation, using the metallizer
258 BaltecMED020 (Leica Microsystemes SAS, France). A Hitachi S800 SEM (Vélizy-
259 Villacoublay, France) with an acceleration voltage of 10 kV and a Zeiss MEB Zeiss Merlin
260 Compact SEM (Marly Le Roi, France) with an acceleration voltage of 2 kV were used to
261 observe particles morphology.
262
263 2.9. High resolution structure determination by TEM observation
264 Formulations were assessed via conventional TEM for further structural characterization
265 (Philips CM120). The polymeric concentration of the analyzed particulate suspension was 26

mg/ml. Both blank PLA-NP and Pam_3CSK_4-loaded PLA-NP (180 µg/mL ligand concentration) were assessed after negative staining by sodium silicotungstate for contrast. Minimum magnification was x40K and maximum magnification was x88K. Size and particle distribution were assessed via ImageJ software.

2.10. Statistical analyses

Statistical analyses were performed using GraphPad Prism Version 6.0 software. All of the data are presented as the mean ± SD. Differences between groups were analyzed as described in figure legends.

3. Results

3.1. PLA-NP characteristics

According to the nanoprecipitation process described in material and methods, PLA-NP synthetized with water or with carbonate buffer as the aqueous phase showed an average hydrodynamic diameter of 190 and 149 nm, and a zeta potential of -59 and -63 mV respectively. The composition of aqueous phase therefore influenced the PLA-NP characteristics as the size decreased by 30%. Concerning Pam_3CSK_4-NP, nanoprecipitation with water in aqueous phase was not achievable. For instance, carbonate buffer was used. The vectorization of the molecule did not modify the colloidal morphological parameters, regardless of the incorporated quantity. All formulations (blank and Pam_3CSK_4-loaded PLA-NP) were prepared in a reproducible manner (three different batches per evaluated concentration) and are stable for at least 30 days (data not shown). Nanoprecipitation process provides monodisperse suspension (PDI<0.15). The final Pam_3CSK_4 concentration loaded into PLA-NP was in a 40 - 180 µg/mL range for a targeted PLA-NP diameter of approximately 150 nm (Table 1). All formulations contained approximatively 10^{12} NP/mL.

The ability of the supernatants to stimulate TLR2 was tested *in vitro* to detect the Pam_3CSK_4 that remained in free-form in our particulate suspensions. All supernatants show a minor

optical density when compared to the control. It indicates that TLR2 activation is significantly lower than the activation triggered by a 100 ng/mL solution of free TLR ligand, for each supernatant (Fig. 1). This justifies the quantity of unloaded Pam_3CSK_4 is negligible, revealing an entrapment efficiency of Pam_3CSK_4 of more than 99%. The optical densities of MAb-TLR2 and unstimulated control are similar, showing that MAb-TLR2 significantly blocks NF-KB activation in cells by Pam_3CSK_4. Thus, detected activation is specific to the molecule.

Electron microscopic observations reveal visible heterogeneity dispersion (Fig 2) and decreased particular size. More precisely, TEM acquisitions show a diameter of 157 and 134 nm for blank PLA-NP and Pam_3CSK_4-loaded PLA-NP respectively, namely a 25% reduction of size compared to the one detected via DLS (Table 1). Otherwise, we can also observe in TEM figures several white patches in both suspensions (three in Fig 2C, a dozen in Fig 2D). This is probably due to the superposition of two particles during sample preparation modifying the image contrast, and not due to Pam_3CSK_4 aggregates, since blank NP showed the same image.

3.2. Pam_3CSK_4-loaded PLA-NP activate TLR2 *in vitro*

The immune property of all NP formulations on the TLR2 activation versus free ligand was explored on HEK-Blue™-hTLR2 cells (Fig. 3). Data shows that 10 hours after incubation, Pam_3CSK_4 (dashed line) is a stronger activator compared to the PLA-NP form. This is explained by the direct availability of the free drug and therefore its immediate action. Most importantly, Pam_3CSK_4 remains active after vectorization (solid line). TLR2 activation is proportional to the loaded concentration, indicating that the immunologic potency increases while the PLA-NP properties remain unchanged (see Table 1). Additionally, the PLA-NP did not induce TLR2 activation (dotted line), suggesting that the empty polymeric vector in these conditions (from 1000 to 50 000 NP/cell) have no effect on NF-kB transcription factor.

Next, the TLR2 activation was deduced via optical density estimation for each formulation serie according to their Pam_3CSK_4 concentration (see Table 1). Based on the standard curve equation obtained from the calibration range (as indicated in 2.6), the theoretical BD was

evaluated and compared to experimental data. Surprisingly, the BD% of loaded Pam_3CSK_4 is repeatedly 30%, for all the formulations except batch 1 at 22% (Fig. 4). Vectorizing the ligand therefore impacts its total availability for receptor recognition. Ten hours after incubation, 30% of the theoretical quantity of Pam_3CSK_4 has activated the TLR2, suggesting that another 70% is accessible for future immune stimulation after endocytosis. Free Pam_3CSK_4 was used as positive control (blue bar), where BD% was 99% and TLR2 activation was at least 3 fold higher than tested candidates. Free Pam_3CSK_4 in presence of MAb-TLR2 (red bar) was used as negative control and BD% was 2%.

3.3. PLA polymer/ Pam_3CSK_4 interactions by *in silico* simulation

To elucidate the mechanisms responsible for drug/carrier interactions, the expected encounters and resulting bounds in the formulations were estimated by a molecular modeling approach. More precisely, to investigate the behavior of Pam_3CSK_4 in a water/PLA polymer environment during the nanoprecipitation process, we performed DPD simulations using the Material Studio software (Biovia). All computed a_{ij} parameters are resumed in Table S1 (supplementary data). This non-atomistic simulation allows to model system sizes from nm to µm and is particularly well-adapted to PLA-NP investigations. It uses beads, which represent a moiety or a group of several molecules like water. PLA polymer, water and Pam_3CSK_4 were set up as different types of beads and all parameters were computed (Fig. 5). In order to understand our system and avoid creating a starting point with an *a priori*, an 85 Å radius droplet was formed with a mixture of PLA chains and Pam_3CSK_4 molecules. A layer of water around the droplet was set up to avoid interactions between the droplet and its replicative image. Our system was set at a 600/1 or 600/9 ratio of PLA polymer/ Pam_3CSK_4. At the very start of the simulations, the PLA polymer chains undergo a volume contraction and release all the Pam_3CSK_4 molecules outside of the formed PLA smooth spherical particle. Water molecules are rapidly excluded as well. As a result, no Pam_3CSK_4 or water molecules were found inside the PLA particle. All Pam_3CSK_4 molecules were interacting with the PLA particle by the fatty acid beads (F) and keep interacting during

the whole dynamic simulations. For the highest molecule concentration system, Pam_3CSK_4 make clusters on the PLA particle. These clusters are composed by 2 or 3 molecules and are randomly distributed on the surface of the particle. A close analysis of the interface reveals that the F beads seem to mix with the first and second layer of PLA monomers (LA) on the surface, suggesting that the interaction is important. Fatty acid chains are in bulky and nonlinear conformations, spreading partially on the surface (Fig. 6).

4. Discussion

Nanotechnologies are promising immunotherapies as they offer tools to protect therapeutic molecules from endogenous degradation, deliver it in specific organ or cell type, and avoid the well documented and too frequent side effects of immune modulators. Previous studies have already highlighted these advantages of immune agonists incorporation into nanovectors to improve their uptake and thus, the defense response (Getts et al., 2015) (Uto et al., 2009).

Here, we successfully entrap the TLR1/2 ligand Pam_3CSK_4 into PLA-NP even at concentrations above the CAC, in a stable and reproducible manner, and we provide molecular clues to explain such results. Carbonate buffer (5mM) added in the aqueous phase during formulation enables the previously unachievable vectorization. More precisely, the buffer provokes a pH shift up to the isoelectric point of the molecule (pI=11, computational predictions). Thus, the environment is in favor of amphiphilic molecule/hydrophobic polymer interactions rather than repulsion and self-assembling. Furthermore, PLA-NP diameter decreased when water was replaced with carbonate buffer in production process, for both blank and Pam_3CSK_4-loaded PLA-NP (see Table 1). This phenomenon is most probably due to ionic forces brought by the buffer against PLA polymers, seeing as the carbonate charges are absent in water. We also noticed the slight intra-batch size decrease between spectroscopy and electron microscopy (see DLS and TEM results for batches A and 5 in Table 1). DLS is an intensity-based technique and uses

solvated samples, whereas TEM is a number-based one and uses dried samples, that explains the 25% size difference between both (Bhattacharjee, 2016).

Concerning the Pam_3CSK_4 loading in PLA-NP, the maximum concentration was 180 µg/mL, for a constant PLA-NP diameter (approximately 150 nm, see Table 1), with >99% entrapment rate, whereas the CAC is 30 µg/mL. We related this observation with *in silico* predictions about PLA polymer/Pam_3CSK_4 fatty acid chains interactions. In presence of PLA polymer, Pam_3CSK_4 interacts with it by stable hydrophobic bounds instead of self-assembling. This competition shifts the CAC towards a higher value via formation of Pam_3CSK_4 clusters at the surface of the particle. Because the frequency of these events are insignificant compared to the particle surface, the diameters and zeta potentials remain unmodified. Attempts to synthesize PLA-NP samples with a concentration over 180 µg/mL of Pam_3CSK_4 were unsuccessful and led to the formation of agglomerates during the nanoprecipitation process. We hypothesize that this is the concentration threshold at which the Pam_3CSK_4 molecules starts self-assembling rather than interacting with PLA molecules. This chemical destabilization would generate Pam_3CSK_4-cluster detachment from the polymer and thus precipitate during NP formulation.

Combined altogether, our performing *in silico* approach and experimental data bring new and original insights regarding the molecular mechanistic of a lipopeptide-derived drug conjugated to a particulate delivery system. For instance, we show that Pam_3CSK_4 is not strictly encapsulated *inside* the PLA-NP but is rather vectorized by them on surface, with the hydrophobic part towards the core and peptidic part outside. Still, the vectorization feasibility using DDS and the high %EE highlighted in our paper corroborate with previous works demonstrating a Pam_3CSK_4 vectorization, in Poly(D,L-lactic-co-glycolic acid) (PLGA) NP (Alkie et al., 2017). In this work, the molecule is adsorbed at the surface (justifying the increased size and zeta potential) through different physicochemical properties of polymer. In another study using liposomes (Bal et al., 2011) the molecule is incorporated into the core, without size and charge modifications.

405 Concerning the *in vitro* immune properties of the different PLA-NP formulations, TLR2
406 binding potential by Pam_3CSK_4 was also explored. Loaded forms showed 30% of their total
407 theoretical capacity to stimulate the receptor. The clusterization of Pam_3CSK_4 at the surface
408 of PLA-NP illustrated by molecular modelling does not impact its activity (Fig. 3). Thus, we
409 suppose that approximately 30% of the ligand is active at a given time for a given cell
410 membrane. This dynamic mechanism is in favor of the vectorization of the ligand in order to
411 have a prolonged and sustained immune response when compared to its free form. The
412 molecule will be subject to cell internalization after PLA-NP endocytosis, allowing further
413 bindings after release. The reduced TLR activation by encapsulated Pam_3CSK_4 compared to
414 free form correlates with the fact that TLR2 is expressed on the cell surface. Conceivably,
415 free Pam_3CSK_4 can directly interact with its receptor. When loaded onto PLA-NP, part of the
416 three chains are available on the outside, as proposed by the model on Fig. 6. Furthermore,
417 it is important to note that after binding to its receptor, an important step will occur after
418 endocytosis. This could delay TLR2 activation, as it reduces Pam_3CSK_4 interactions with
419 surface cell, that will happen later in the endosome. We compared such observations to prior
420 data we got concerning *in vitro* cytosolic activation of TLR9 with free and loaded TLR9
421 agonist form (CpG molecule). Interestingly, these CpG-loaded PLA-NP were more efficient
422 during intracellular activation than soluble form (data not shown). Thus, PLA-NP improve
423 cellular ligand entrapment, which corroborates with our present hypothesis about
424 extracellular TLR2 activation delay and molecular modelling adsorption indicating the
425 presence of Pam_3CSK_4 as a cluster-corona partially surrounding the PLA-NP.
426 While PLA undergoes hydrolysis after endocytosis and produces lactate monomers that
427 enters the host's metabolic pathways, Pam_3CSK_4 molecules are recycled to the cell
428 membrane to stimulate the TLR1/2 ligands once again. This active dynamism maintained via
429 PLA-NP vectorization would ultimately improve the potency and duration of the expected
430 immune response. *In vitro* experiments have some limit to prove this all body dynamism,
431 therefore *in vivo* investigations are in progress to demonstrate the prolonged immune effect
432 of Pam_3CSK_4-loaded PLA-NP. In the same vein, *in vitro* cytotoxicity is routinely evaluated for

any given drug under development. However, immune-mediated adverse effects may occur in humans after systemic administration of pharmaceutical products and particularly immune modulators. Such phenomenons are classified under the broad spectrum of infusion reactions (Szebeni et al., 2018). For these reasons, animal studies are essential in order to assert the definite safe-by-design profile of NP (Zamboni et al., 2018). Thus, to verify the biodistribution of our vectors, further *in vivo* investigations are in progress. The present study brings highly valuable precisions about PLA-NP surface identity that will help anticipate pharmacokinetic studies and side effects. Recent reports have been disclosing how NP surface properties significantly affect their interaction with cells. This interesting corona characteristic proper to nanovectors will surely participate to the full unravelling of their structure-activity relationship (Bertrand et al., 2017).

5. Conclusions

In this study, we investigated the loading mechanisms of TLR1/2 ligand onto PLA-NP, using both biochemistry approaches and molecular modelling tools. Such information has led us to obtain reproducible and stable Pam_3CSK_4-loaded PLA-NP formulations, illustrating the added value of PLA-NP as a delivery system for immunotherapies. The nanoprecipitation method led us to produce batches in a simple manner without toxic reagents as surfactants (Martínez Rivas et al., 2017) and stable over time. Furthermore, PLA polymer offer the advantage to be less toxic than inorganic polymers. We overrided the self-assembling phenomenon of the amphiphilic molecule, by adjusting the pH of aqueous phase without affecting the bioactivity of the final product. This method should be applicable to similar lipopeptides and more generally to hydrophobic molecules. Additionally, we took advantage of the innovative molecular modelling approach to understand drug/carrier interactions and thus, to predict experimental expectations. We are able to achieve adapted formulations depending on the needed. For vaccine purpose, encapsulation of immune modulators such as different PRR ligands (Gutjahr et al., 2016) could facilitate antigen presenting cell

stimulation by protecting the molecule and potentializing their activities. For these reasons and seeing as Pam_3CSK_4 does not respect Lipinski's rule of five, vectorizing this particular ligand is all the more justified (Walters, 2012).

Next strategies will be the functionalization of PLA-NP for active targeting of vectors depending on the organ of interest and the route of administration since its dictates the immunogenicity (Sultan et al., 2019). Furthermore, we should emphasize that loading of any molecule will modify the surface chemistry of PLA-NP which could influence their immune-regulation properties as surface charge will be modified, and by consequence their interaction with fluid environment, when injected *in vivo*.

This proof of concept aims to demonstrate that it is possible to encapsulate an immune modulator into PLA biodegradable NP when mastering the biochemical events and the knowledge of molecular interactions involved. The loading process identified in this work does not interfere with the immune properties of Pam_3CSK_4. Furthermore, molecular modelling could bring some mechanistic explanations to the rearrangement of the ligand during the nanoprecipitation process explain its biological properties. This novel DDS and the associate molecular modelling tools are of interest for further applications in immunotherapy, either vaccine of cancer field.

- Conflict of interest

BV declares financial interests in Adjuvatis.

- Acknowledgements

We acknowledge the contribution of SFR Biosciences (UMS3444/CNRS, US8/Inserm, ENS de Lyon, UCBL) for CTμ platform and Christelle Boulé for electron microscopy assistance.

- Author contributions

BV, ML and RT designed the study. ML, FC, SH, SM performed experiments and analyzed data. All authors participated to the writing of the manuscript.

- Funding sources

ML was supported by La Ligue contre le Cancer for three years by PhD studentship. Financial support is gained from ANRS (Agence Nationale de Recherche sur le SIDA et les hépatites virales) and from ANR (French National Research Agency) under the frame of "European Innovative Research & Technological Development Projects in Nanomedicine" within the framework of the ERA-NET, EuroNanoMed-II concerning the FlunanoAir research program, from ANR-16-CE15-0002 (MemoSign) and from ANR-16-CE20-0002-01 (FishRNAVax) to BV.

Alkie, T.N., Taha-Abdelaziz, K., Barjesteh, N., Bavananthasivam, J., Hodgins, D.C., Sharif, S., 2017. Characterization of Innate Responses Induced by PLGA Encapsulated- and Soluble TLR Ligands In Vitro and In Vivo in Chickens. PLoS ONE 12, e0169154. https://doi.org/10.1371/journal.pone.0169154

Bal, S.M., Hortensius, S., Ding, Z., Jiskoot, W., Bouwstra, J.A., 2011. Co-encapsulation of antigen and Toll-like receptor ligand in cationic liposomes affects the quality of the immune response in mice after intradermal vaccination. Vaccine 29, 1045–1052. https://doi.org/10.1016/j.vaccine.2010.11.061

Banik, B.L., Fattahi, P., Brown, J.L., 2016. Polymeric nanoparticles: the future of nanomedicine. Wiley Interdisciplinary Reviews: Nanomedicine and Nanobiotechnology 8, 271–299. https://doi.org/10.1002/wnan.1364

Beeh, K.-M., Kanniess, F., Wagner, F., Schilder, C., Naudts, I., Hammann-Haenni, A., Willers, J., Stocker, H., Mueller, P., Bachmann, M.F., Renner, W.A., 2013. The novel TLR-9 agonist QbG10 shows clinical efficacy in persistent allergic asthma. J. Allergy Clin. Immunol. 131, 866–874. https://doi.org/10.1016/j.jaci.2012.12.1561

Behzadi, S., Serpooshan, V., Tao, W., Hamaly, M.A., Alkawareek, M.Y., Dreaden, E.C., Brown, D., Alkilany, A.M., Farokhzad, O.C., Mahmoudi, M., 2017. Cellular Uptake of Nanoparticles: Journey Inside the Cell. Chem Soc Rev 46, 4218–4244. https://doi.org/10.1039/c6cs00636a

Bertrand, N., Grenier, P., Mahmoudi, M., Lima, E.M., Appel, E.A., Dormont, F., Lim, J.-M., Karnik, R., Langer, R., Farokhzad, O.C., 2017. Mechanistic understanding of in vivo protein corona formation on polymeric nanoparticles and impact on pharmacokinetics. Nat Commun 8, 777. https://doi.org/10.1038/s41467-017-00600-w

Bhattacharjee, S., 2016. DLS and zeta potential - What they are and what they are not? J Control Release 235, 337–351. https://doi.org/10.1016/j.jconrel.2016.06.017

Boisgard, A.-S., Lamrayah, M., Dzikowski, M., Salmon, D., Kirilov, P., Primard, C., Pirot, F., Fromy, B., Verrier, B., 2017. Innovative drug vehicle for local treatment of inflammatory skin diseases: Ex vivo and in vivo screening of five topical formulations containing poly(lactic acid) (PLA) nanoparticles. Eur J Pharm Biopharm 116, 51–60. https://doi.org/10.1016/j.ejpb.2016.09.021

Boni, C., Vecchi, A., Rossi, M., Laccabue, D., Giuberti, T., Alfieri, A., Lampertico, P., Grossi, G., Facchetti, F., Brunetto, M.R., Coco, B., Cavallone, D., Mangia, A., Santoro, R., Piazzolla, V., Lau, A., Gaggar, A., Subramanian, G.M., Ferrari, C., 2018. TLR7 Agonist Increases Responses of Hepatitis B Virus-Specific T Cells and Natural Killer

Cells in Patients With Chronic Hepatitis B Treated With Nucleos(T)Ide Analogues. Gastroenterology 154, 1764-1777.e7. https://doi.org/10.1053/j.gastro.2018.01.030
Botos, I., Segal, D.M., Davies, D.R., 2011. The Structural Biology of Toll-Like Receptors. Structure 19, 447–459. https://doi.org/10.1016/j.str.2011.02.004
Chow, L.Q.M., Morishima, C., Eaton, K.D., Baik, C.S., Goulart, B.H., Anderson, L.N., Manjarrez, K.L., Dietsch, G.N., Bryan, J.K., Hershberg, R.M., Disis, M.L., Martins, R.G., 2017. Phase Ib Trial of the Toll-like Receptor 8 Agonist, Motolimod (VTX-2337), Combined with Cetuximab in Patients with Recurrent or Metastatic SCCHN. Clin. Cancer Res. 23, 2442–2450. https://doi.org/10.1158/1078-0432.CCR-16-1934
Coler, R.N., Day, T.A., Ellis, R., Piazza, F.M., Beckmann, A.M., Vergara, J., Rolf, T., Lu, L., Alter, G., Hokey, D., Jayashankar, L., Walker, R., Snowden, M.A., Evans, T., Ginsberg, A., Reed, S.G., TBVPX-113 Study Team, 2018. The TLR-4 agonist adjuvant, GLA-SE, improves magnitude and quality of immune responses elicited by the ID93 tuberculosis vaccine: first-in-human trial. NPJ Vaccines 3, 34. https://doi.org/10.1038/s41541-018-0057-5
Coolen, A.-L., Lacroix, C., Mercier-Gouy, P., Delaune, E., Monge, C., Exposito, J.-Y., Verrier, B., 2019. Poly(lactic acid) nanoparticles and cell-penetrating peptide potentiate mRNA-based vaccine expression in dendritic cells triggering their activation. Biomaterials 195, 23–37. https://doi.org/10.1016/j.biomaterials.2018.12.019
Dalzon, B., Lebas, C., Jimenez, G., Gutjahr, A., Terrat, C., Exposito, J.-Y., Verrier, B., Lethias, C., 2016. Poly(Lactic Acid) Nanoparticles Targeting α5β1 Integrin as Vaccine Delivery Vehicle, a Prospective Study. PLoS ONE 11, e0167663. https://doi.org/10.1371/journal.pone.0167663
Dong, P., Rakesh, K.P., Manukumar, H.M., Mohammed, Y.H.E., Karthik, C.S., Sumathi, S., Mallu, P., Qin, H.-L., 2019. Innovative nano-carriers in anticancer drug delivery-a comprehensive review. Bioorg. Chem. 85, 325–336. https://doi.org/10.1016/j.bioorg.2019.01.019
Engel, A.L., Holt, G.E., Lu, H., 2011. The pharmacokinetics of Toll-like receptor agonists and the impact on the immune system. Expert Rev Clin Pharmacol 4, 275–289. https://doi.org/10.1586/ecp.11.5
Getts, D.R., Shea, L.D., Miller, S.D., King, N.J.C., 2015. Harnessing nanoparticles for immune modulation. Trends Immunol 36, 419–427. https://doi.org/10.1016/j.it.2015.05.007
Gutjahr, A., Phelip, C., Coolen, A.-L., Monge, C., Boisgard, A.-S., Paul, S., Verrier, B., 2016. Biodegradable Polymeric Nanoparticles-Based Vaccine Adjuvants for Lymph Nodes Targeting. Vaccines (Basel) 4. https://doi.org/10.3390/vaccines4040034
Hamley, I.W., Kirkham, S., Dehsorkhi, A., Castelletto, V., Reza, M., Ruokolainen, J., 2014. Toll-like receptor agonist lipopeptides self-assemble into distinct nanostructures. Chem. Commun. 50, 15948–15951. https://doi.org/10.1039/C4CC07511K
Hennessy, E.J., Parker, A.E., O'Neill, L.A.J., 2010. Targeting Toll-like receptors: emerging therapeutics? Nat Rev Drug Discov 9, 293–307. https://doi.org/10.1038/nrd3203
Ignacio, B.J., Albin, T.J., Esser-Kahn, A.P., Verdoes, M., 2018. Toll-like Receptor Agonist Conjugation: A Chemical Perspective. Bioconjug. Chem. 29, 587–603. https://doi.org/10.1021/acs.bioconjchem.7b00808
Khan, S., Weterings, J.J., Britten, C.M., de Jong, A.R., Graafland, D., Melief, C.J.M., van der Burg, S.H., van der Marel, G., Overkleeft, H.S., Filippov, D.V., Ossendorp, F., 2009. Chirality of TLR-2 ligand Pam3CysSK4 in fully synthetic peptide conjugates critically influences the induction of specific CD8+ T-cells. Mol. Immunol. 46, 1084–1091. https://doi.org/10.1016/j.molimm.2008.10.006
Kim, C., Rockenstein, E., Spencer, B., Kim, H.-K., Adame, A., Trejo, M., Stafa, K., Lee, H.-J., Lee, S.-J., Masliah, E., 2015. Antagonizing Neuronal Toll-like Receptor 2 Prevents Synucleinopathy by Activating Autophagy. Cell Rep 13, 771–782. https://doi.org/10.1016/j.celrep.2015.09.044

Lamalle-Bernard, D., Munier, S., Compagnon, C., Charles, M.-H., Kalyanaraman, V.S., Delair, T., Verrier, B., Ataman-Onal, Y., 2006. Coadsorption of HIV-1 p24 and gp120 proteins to surfactant-free anionic PLA nanoparticles preserves antigenicity and immunogenicity. J Control Release 115, 57–67. https://doi.org/10.1016/j.jconrel.2006.07.006

Lang, K.S., Recher, M., Junt, T., Navarini, A.A., Harris, N.L., Freigang, S., Odermatt, B., Conrad, C., Ittner, L.M., Bauer, S., Luther, S.A., Uematsu, S., Akira, S., Hengartner, H., Zinkernagel, R.M., 2005. Toll-like receptor engagement converts T-cell autoreactivity into overt autoimmune disease. Nature Medicine 11, 138. https://doi.org/10.1038/nm1176

Lee, S.-K., Chwee, J.Y., Ma, C.A.P., Bert, N.L., Huang, C.W., Gasser, S., 2014. Synergistic Anticancer Effects of Pam3CSK4 and Ara-C on B-Cell Lymphoma Cells. Clin Cancer Res 20, 3485–3495. https://doi.org/10.1158/1078-0432.CCR-13-2522

Legaz, S., Exposito, J.-Y., Lethias, C., Viginier, B., Terzian, C., Verrier, B., 2016. Evaluation of polylactic acid nanoparticles safety using Drosophila model. Nanotoxicology 10, 1136–1143. https://doi.org/10.1080/17435390.2016.1181806

Li, J.-K., Balic, J.J., Yu, L., Jenkins, B., 2017. TLR Agonists as Adjuvants for Cancer Vaccines, in: Xu, D. (Ed.), Regulation of Inflammatory Signaling in Health and Disease, Advances in Experimental Medicine and Biology. Springer Singapore, Singapore, pp. 195–212. https://doi.org/10.1007/978-981-10-5987-2_9

Lucifora, J., Bonnin, M., Aillot, L., Fusil, F., Maadadi, S., Dimier, L., Michelet, M., Floriot, O., Ollivier, A., Rivoire, M., Ait-Goughoulte, M., Daffis, S., Fletcher, S.P., Salvetti, A., Cosset, F.-L., Zoulim, F., Durantel, D., 2018. Direct antiviral properties of TLR ligands against HBV replication in immune-competent hepatocytes. Sci Rep 8, 5390. https://doi.org/10.1038/s41598-018-23525-w

Martínez Rivas, C.J., Tarhini, M., Badri, W., Miladi, K., Greige-Gerges, H., Nazari, Q.A., Galindo Rodríguez, S.A., Román, R.Á., Fessi, H., Elaissari, A., 2017. Nanoprecipitation process: From encapsulation to drug delivery. Int J Pharm 532, 66–81. https://doi.org/10.1016/j.ijpharm.2017.08.064

Miernicki, M., Hofmann, T., Eisenberger, I., Kammer, F. von der, Praetorius, A., 2019. Legal and practical challenges in classifying nanomaterials according to regulatory definitions. Nature Nanotechnology 14, 208. https://doi.org/10.1038/s41565-019-0396-z

Mifsud, E.J., Tan, A.C.-L., Jackson, D.C., 2014. TLR Agonists as Modulators of the Innate Immune Response and Their Potential as Agents Against Infectious Disease. Front. Immunol. 5. https://doi.org/10.3389/fimmu.2014.00079

Pavot, V., Rochereau, N., Primard, C., Genin, C., Perouzel, E., Lioux, T., Paul, S., Verrier, B., 2013. Encapsulation of Nod1 and Nod2 receptor ligands into poly(lactic acid) nanoparticles potentiates their immune properties. J Control Release 167, 60–67. https://doi.org/10.1016/j.jconrel.2013.01.015

Peres, C., Matos, A.I., Conniot, J., Sainz, V., Zupančič, E., Silva, J.M., Graça, L., Sá Gaspar, R., Préat, V., Florindo, H.F., 2017. Poly(lactic acid)-based particulate systems are promising tools for immune modulation. Acta Biomaterialia 48, 41–57. https://doi.org/10.1016/j.actbio.2016.11.012

Ragelle, H., Danhier, F., Préat, V., Langer, R., Anderson, D.G., 2017. Nanoparticle-based drug delivery systems: a commercial and regulatory outlook as the field matures. Expert Opin Drug Deliv 14, 851–864. https://doi.org/10.1080/17425247.2016.1244187

Reed, S.G., Orr, M.T., Fox, C.B., 2013. Key roles of adjuvants in modern vaccines. Nature Medicine 19, 1597–1608. https://doi.org/10.1038/nm.3409

Rességuier, J., Delaune, E., Coolen, A.-L., Levraud, J.-P., Boudinot, P., Le Guellec, D., Verrier, B., 2017. Specific and Efficient Uptake of Surfactant-Free Poly(Lactic Acid) Nanovaccine Vehicles by Mucosal Dendritic Cells in Adult Zebrafish after Bath Immersion. Front Immunol 8, 190. https://doi.org/10.3389/fimmu.2017.00190

Riley, R.S., June, C.H., Langer, R., Mitchell, M.J., 2019. Delivery technologies for cancer immunotherapy. Nat Rev Drug Discov 18, 175–196. https://doi.org/10.1038/s41573-018-0006-z

Sultan, H., Kumai, T., Nagato, T., Wu, J., Salazar, A.M., Celis, E., 2019. The route of administration dictates the immunogenicity of peptide-based cancer vaccines in mice. Cancer Immunol. Immunother. 68, 455–466. https://doi.org/10.1007/s00262-018-02294-5

Szebeni, J., Simberg, D., González-Fernández, Á., Barenholz, Y., Dobrovolskaia, M.A., 2018. Roadmap and strategy for overcoming infusion reactions to nanomedicines. Nat Nanotechnol 13, 1100–1108. https://doi.org/10.1038/s41565-018-0273-1

Tacken, P.J., Zeelenberg, I.S., Cruz, L.J., van Hout-Kuijer, M.A., van de Glind, G., Fokkink, R.G., Lambeck, A.J.A., Figdor, C.G., 2011. Targeted delivery of TLR ligands to human and mouse dendritic cells strongly enhances adjuvanticity. Blood 118, 6836–6844. https://doi.org/10.1182/blood-2011-07-367615

Tyler, B., Gullotti, D., Mangraviti, A., Utsuki, T., Brem, H., 2016. Polylactic acid (PLA) controlled delivery carriers for biomedical applications. Advanced Drug Delivery Reviews, PLA biodegradable polymers 107, 163–175. https://doi.org/10.1016/j.addr.2016.06.018

Uto, T., Akagi, T., Hamasaki, T., Akashi, M., Baba, M., 2009. Modulation of innate and adaptive immunity by biodegradable nanoparticles. Immunol. Lett. 125, 46–52. https://doi.org/10.1016/j.imlet.2009.05.008

Walters, W.P., 2012. Going further than Lipinski's rule in drug design. Expert Opinion on Drug Discovery 7, 99–107. https://doi.org/10.1517/17460441.2012.648612

Zamboni, W.C., Szebeni, J., Kozlov, S.V., Lucas, A.T., Piscitelli, J.A., Dobrovolskaia, M.A., 2018. Animal models for analysis of immunological responses to nanomaterials: Challenges and considerations. Adv. Drug Deliv. Rev. 136–137, 82–96. https://doi.org/10.1016/j.addr.2018.09.012

Zhao, S., Gao, N., Qi, H., Chi, H., Liu, B., He, B., Wang, J., Jin, Z., He, X., Zheng, H., Wang, Z., Wang, X., Jin, G., 2019. Suppressive effects of sunitinib on a TLR activation-induced cytokine storm. European Journal of Pharmacology 854, 347–353. https://doi.org/10.1016/j.ejphar.2019.04.045

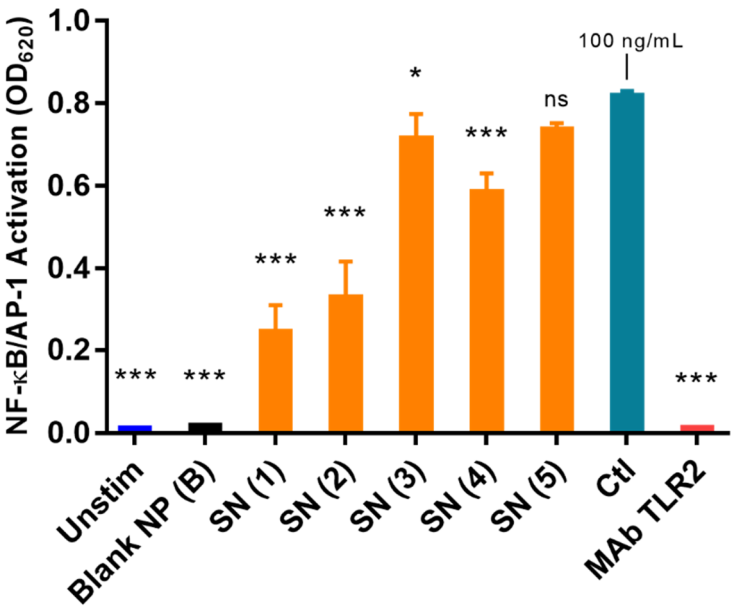

Fig. 1: Quantification of the free Pam_3CSK_4 fraction of each PLA-NP formulation via quantification of the TLR2 activation by the supernatants. Results are represented as mean±SD of three independent experiments. ***p<0.001, *p<0.05, ns: not significant (p>0.05) by one-way ANOVA with Dunnett post test correction. Asterisks indicate statistically significant differences between the control (free Pam_3CSK_4 at 100 ng/mL).

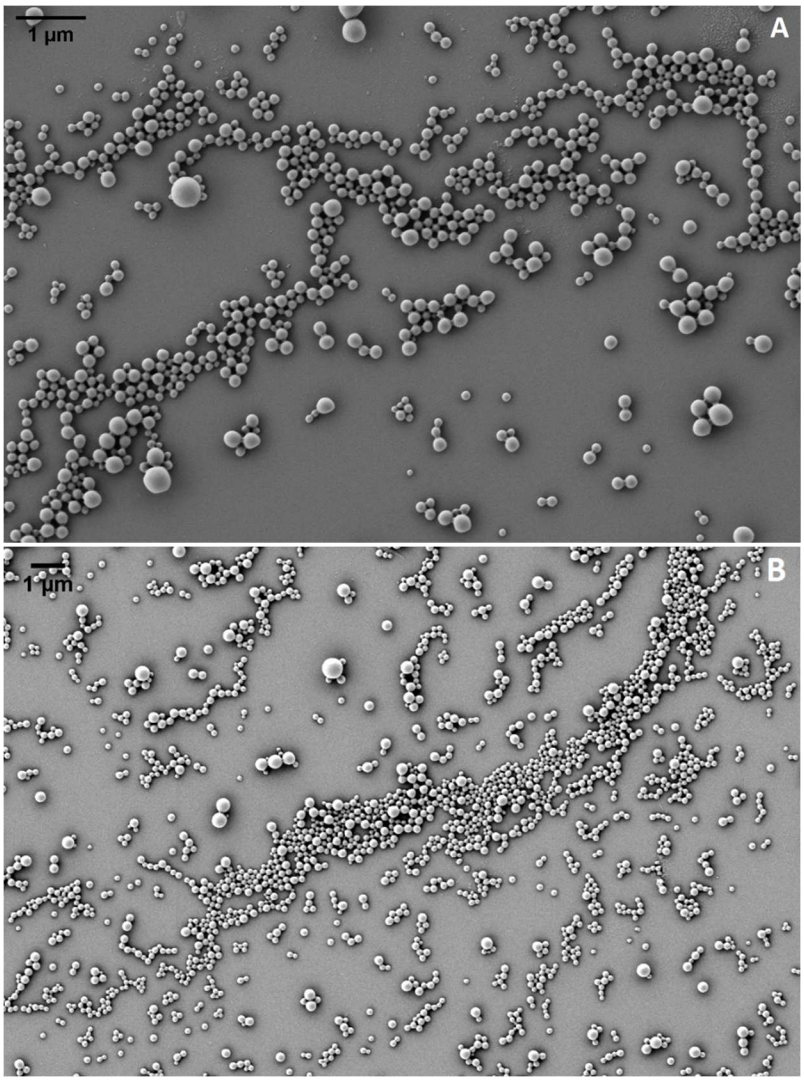
1 µm
A
1 µm
B

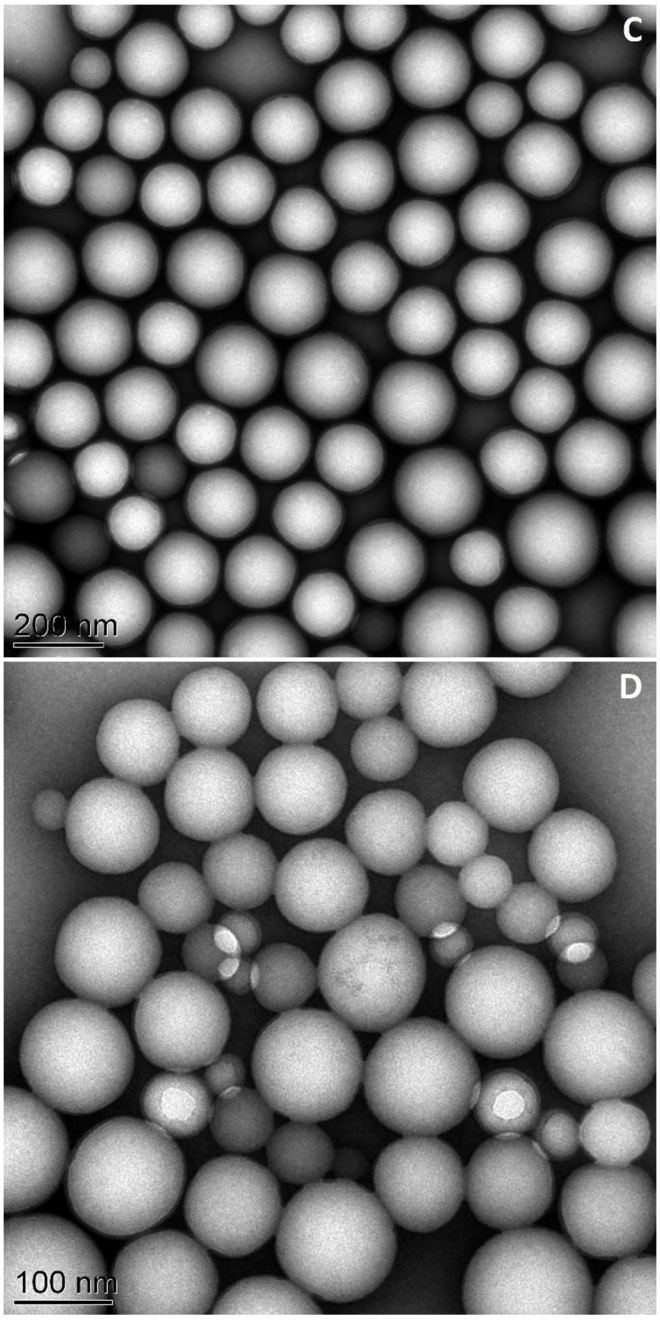

Fig. 2: Electron microscopy images of blank PLA-NP (A) and Pam_3CSK_4 PLA-NP (B) by SEM and blank PLA-NP (C) and Pam_3CSK_4 PLA-NP (D) by TEM (scale bar in each image).

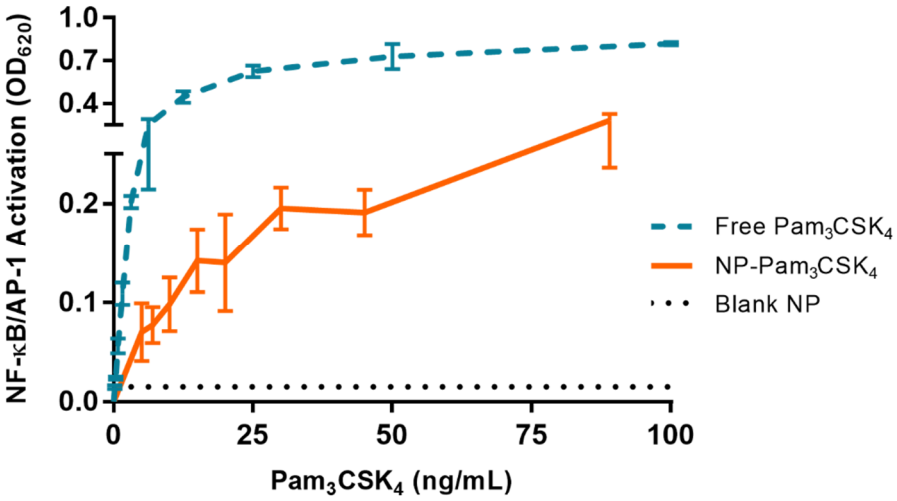

Fig. 3: TLR2-activating efficiency of free Pam_3CSK_4 (blue) and Pam_3CSK_4 loaded in PLA-NP (orange) in HEK-Blue™-hTLR2 cells. Blank NP are used as negative control (black). Absorbance is measured 10 hours after cell incubation. Data are mean±SD of three independent experiments.

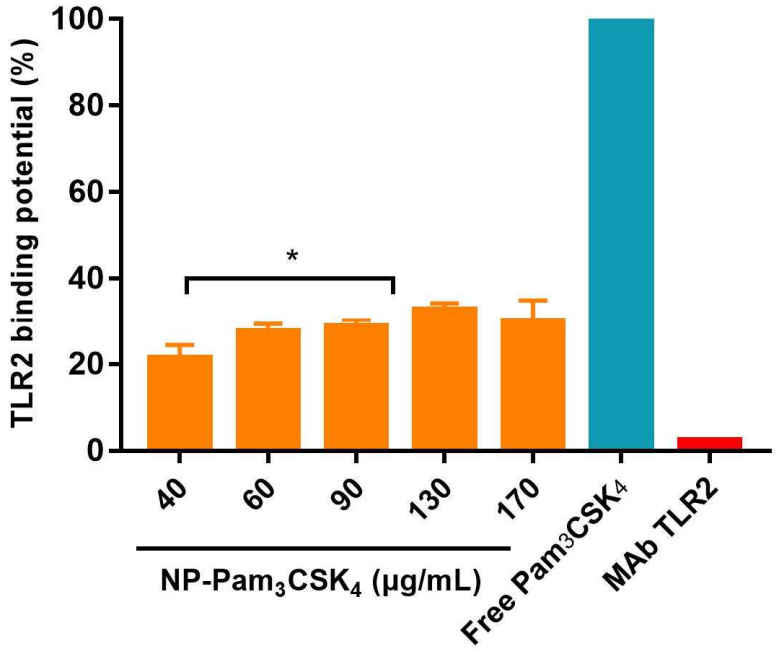

Fig. 4: TLR2 activation efficiency by each PLA-NP formulation. Free Pam_3CSK_4 was used as positive control (blue). Data are mean±SD of three independent experiments. *$p<0.05$, by one-way ANOVA with Dunnett post test correction. The other comparisons between Total (x) bars were not significantly different.

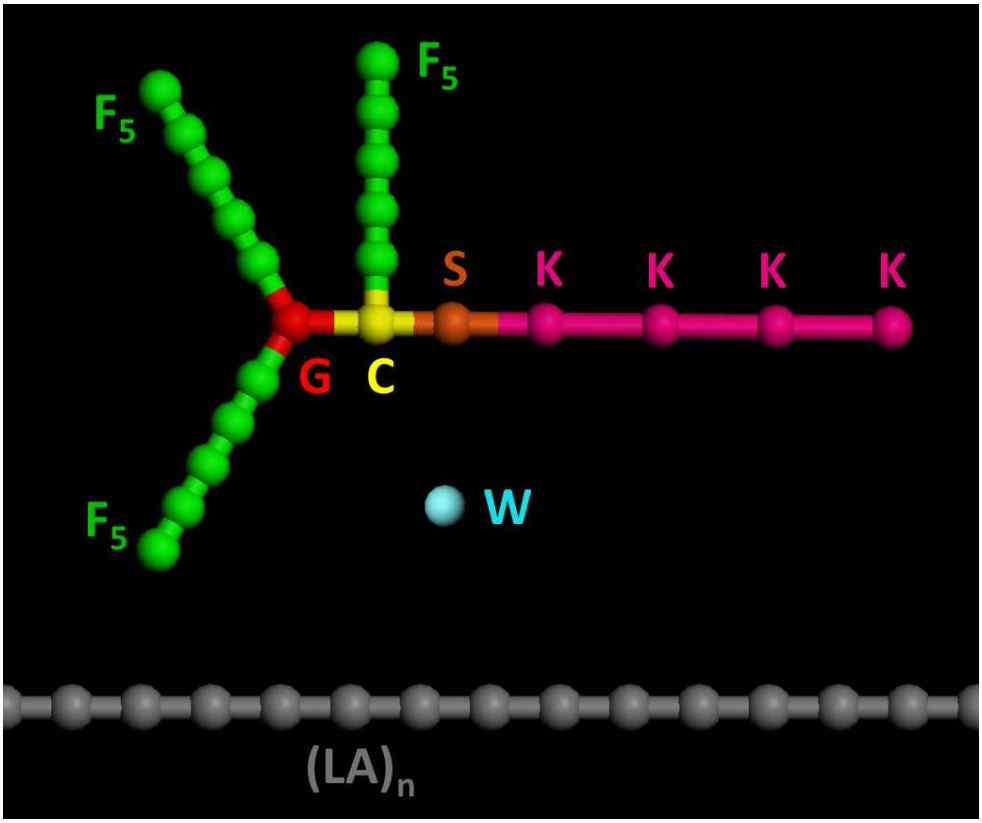

Fig. 5 Schematic representation of the 7 different kinds of beads used for the DPD calculations. Lysine (K), Serine (S), modified Cysteine (C), modified Glycerol (G), and C_3H_6 fatty acid units (F) for Pam_3CSK_4, linear chains of Lactic Acid monomers $(LA)_n$ for PLA, and Water (W), where one bead represents 3 molecules of water.

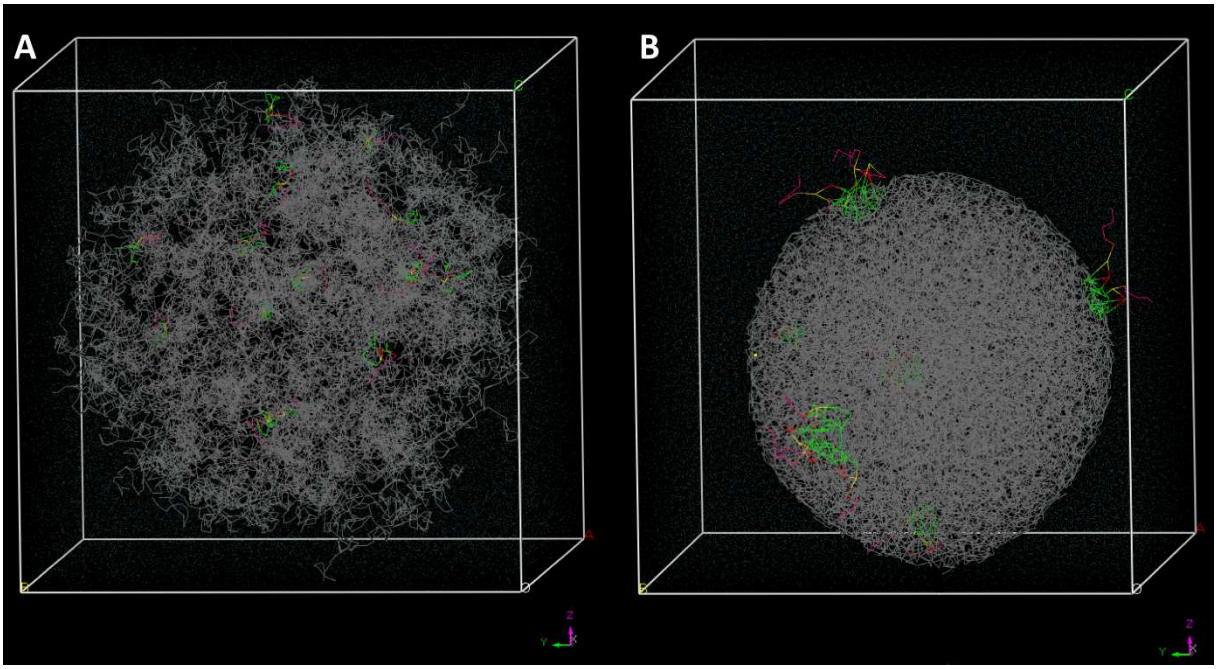

Fig. 6: DPD simulation: with the starting point (A) where a droplet with a radius of 85 Å containing a mixture of PLA and Pam_3CSK_4 molecules is placed at the center of a water-filled simulation box; and after 30 ns total simulation time (B) where Pam_3CSK_4 molecules are excluded from the PLA-NP and form clusters, which interact with the surface through their fatty acid chains (F). The Pam_3CSK_4:PLA ratio is 0.4% (w/w).

NP batches	Loaded Pam_3CSK_4 (µg/mL)	Aqueous phase during NP formulation	Diameter (nm)		Zeta potential (mV)	Dispersity (PDI)
			DLS	TEM		
Blank NP (A)	0	Water	190 ±2	157±17	-59 ±4	0.049 ±0.015
Blank NP (B)	0	Na_2CO_3 5 mM	149 ±4	NA	-63 ±1	0.102 ±0.016
NP- Pam_3CSK_4 (1)	43 ±3	Na_2CO_3 5 mM	147 ±3	NA	-59 ±1	0.098 ±0.030
NP- Pam_3CSK_4 (2)	63 ±4	Na_2CO_3 5 mM	147 ±5	NA	-60 ±4	0.121 ±0.029
NP- Pam_3CSK_4 (3)	94 ±8	Na_2CO_3 5 mM	154 ±9	NA	-63 ±2	0.099 ±0.014
NP- Pam_3CSK_4 (4)	131 ±12	Na_2CO_3 5 mM	153 ±4	NA	-63 ±5	0.108 ±0.009
NP- Pam_3CSK_4 (5)	172 ±10	Na_2CO_3 5 mM	156 ±2	134±18	-66 ±5	0.093 ±0.008

Table 1: Chemical and colloidal characteristics of PLA-NP formulations. Each was performed in triplicate. Results are represented as mean±SD.

1 Formulation of a novel immune modulating delivery system

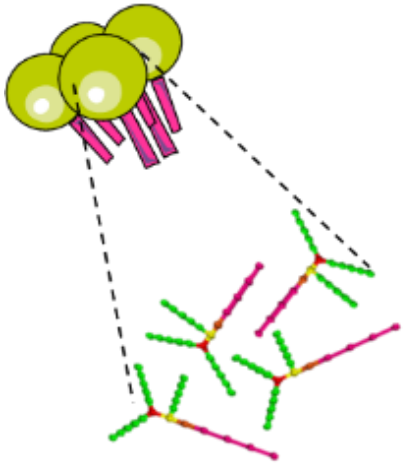

Pam_3CSK_4 molecule as a TLR1/2 ligand

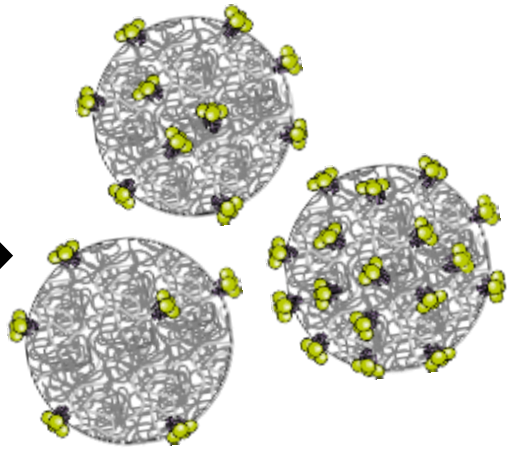

PLA-NP loaded with increasing Pam_3CSK_4 concentrations

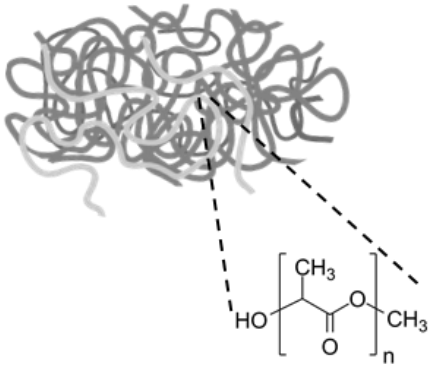

Poly (D,L) Lactic Acid (PLA) for polymeric nanoparticles (NP)

2 Colloidal characterization and molecular modelling of the Pam_3CSK_4-loaded PLA-NP

PLA-NP properties and morphology

- Size and dispersity (by Dynamic Light Scattering)
- Entrapment Efficiency
- Surface morphology (by Electron Microscopy)

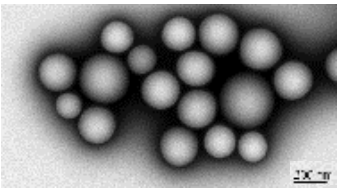

In silico predictions of content-contained dynamics

- Dissipative Particle Dynamics
- Clusters of Pam_3CSK_4 onto PLA-NP surface

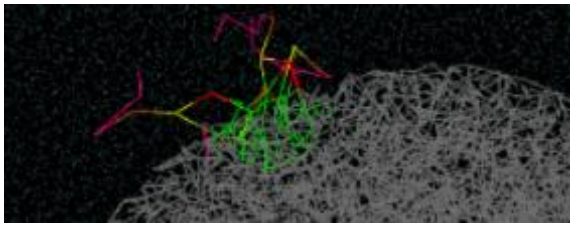

In vitro activity on engineered TLR2 reporter cell line

- Loaded Pam_3CSK_4 remains immunologically active
- Results in favor of a sustained release